AGU PUBLICATIONS

Geophysical Research Letters

RESEARCH LETTER
10.1002/2013GL058819

Special Section:
Early Results from the Van Allen Probes

Event-specific chorus wave and electron seed population models in DREAM3D using the Van Allen Probes

Weichao Tu[1], G. S. Cunningham[1], Y. Chen[1], S. K. Morley[1], G. D. Reeves[1], J. B. Blake[2], D. N. Baker[3], and H. Spence[4]

[1]Space Science and Applications Group, Los Alamos National Laboratory, Los Alamos, New Mexico, USA, [2]Space Sciences Department, The Aerospace Corporation, Los Angeles, California, USA, [3]Laboratory for Atmospheric and Space Physics, University of Colorado Boulder, Boulder, Colorado, USA, [4]Institute for the Study of Earth, Oceans, and Space, University of New Hampshire, Durham, New Hampshire, USA

Key Points:
- DREAM3D uses event-specific driving conditions measured by Van Allen Probes
- Electron dropout is due to outward radial diffusion to compressed magnetopause
- Event-specific chorus and seed electrons are necessary for the enhancement

Correspondence to:
W. Tu,
wtu@lanl.gov

Citation:
Tu, W., G. S. Cunningham, Y. Chen, S. K. Morley, G. D. Reeves, J. B. Blake, D. N. Baker, and H. Spence (2014), Event-specific chorus wave and electron seed population models in DREAM3D using the Van Allen Probes, *Geophys. Res. Lett.*, *41*, doi:10.1002/2013GL058819.

Received 31 DEC 2013
Accepted 29 JAN 2014
Accepted article online 1 FEB 2014

Abstract The DREAM3D diffusion model is applied to Van Allen Probes observations of the fast dropout and strong enhancement of MeV electrons during the October 2012 "double-dip" storm. We show that in order to explain the very different behavior in the two "dips," diffusion in all three dimensions (energy, pitch angle, and L^*) coupled with data-driven, event-specific inputs, and boundary conditions is required. Specifically, we find that outward radial diffusion to the solar wind-driven magnetopause, an event-specific chorus wave model, and a dynamic lower-energy seed population are critical for modeling the dynamics. In contrast, models that include only a subset of processes, use statistical wave amplitudes, or rely on inward radial diffusion of a seed population, perform poorly. The results illustrate the utility of the high resolution, comprehensive set of Van Allen Probes' measurements in studying the balance between source and loss in the radiation belt, a principal goal of the mission.

1. Introduction

The relativistic electron fluxes in Earth's outer radiation belt are observed to vary greatly during geomagnetic storms [*Reeves et al.*, 2003; *X. Li et al.*, 2013]. The successful launch of the Van Allen Probes mission creates an unprecedented opportunity to observe radiation belt dynamics in great detail. During the October 2012 "double-dip" storm event (Figure 1f), the phase space density (PSD) of MeV electrons (shown in Figure 1b) exhibits very different behavior in the two dips: wiped out during the first *Dst* dip and then increased by 3 orders of magnitude on the time scale of hours during the second *Dst* dip. Given that the variability of radiation belt electrons is a delicate balance between various source and loss processes [*Selesnick and Blake*, 2000; *Reeves et al.*, 2003; *Tu et al.*, 2009], understanding the fast dropout and buildup of radiation belt electrons in this event is challenging even with the high-quality particle and wave data from the Van Allen Probes. Physical models are required that can take the highly resolved, comprehensive measurements as inputs.

The fast dropout of radiation belt electrons can be caused by outward radial diffusion combined with magnetopause shadowing [*Reeves et al.*, 1998; *Morley et al.*, 2010; *Shprits et al.*, 2012; *Turner et al.*, 2012] and/or enhanced electron precipitation into the atmosphere [*Selesnick*, 2006; *Tu et al.*, 2010]. The acceleration of radiation belt electrons can be due to inward radial diffusion [*Hudson et al.*, 2000; *Elkington et al.*, 2003] and/or local heating by Very Low Frequency (VLF) waves, such as whistler mode chorus [*Horne and Thorne*, 1998; *Horne et al.*, 2005]. To simulate these concurrent processes, a 3-D model which includes diffusion in all three dimensions (energy, pitch angle, and L^* shell) is needed. Recent data have shown that the electron PSD can peak at L^* regions (L^* is the third adiabatic invariant [*Roederer*, 1970]) inside geosynchronous orbit, leading to a greater emphasis on local heating as the acceleration mechanism for radiation belt electrons [*Chen et al.*, 2007]. For the October 2012 event shown in Figure 1, a detailed analysis of the PSD profiles versus L^* using Van Allen Probes data showed strong evidence of local heating during the second *Dst* dip [*Reeves et al.*, 2013]. Furthermore, a 2-D simulation of the acceleration by chorus waves that reproduces the energy spectrum and pitch angle distributions observed at one L shell has also been performed [*Thorne et al.*, 2013]. In this paper, we complement those recent results by demonstrating that the location of the PSD peak in L is reproduced by DREAM3D, as is the breadth of the distribution in L, and the qualitative features seen during both the first and second *Dst* dips.

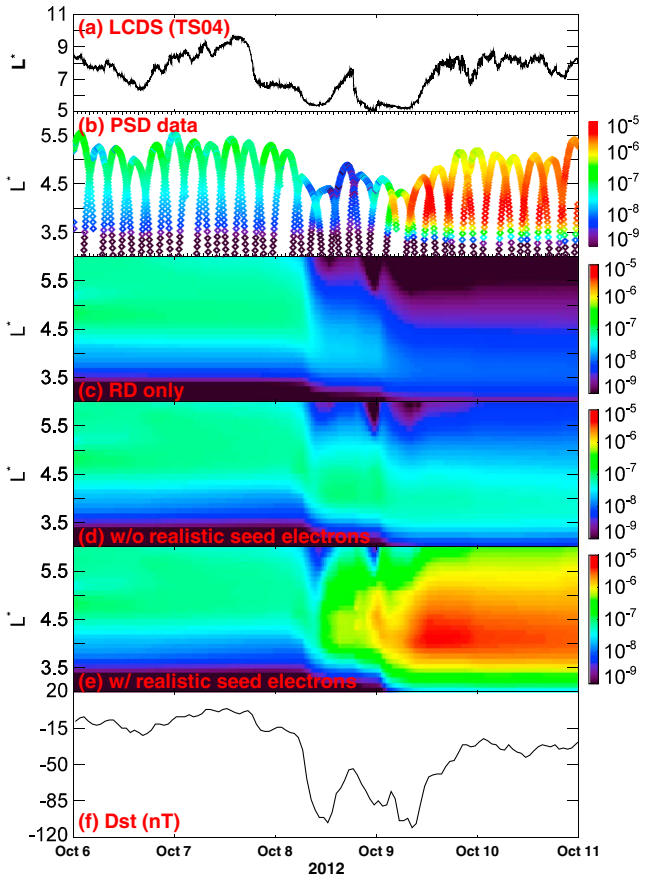

Figure 1. Electron PSD data (in units of $(c/MeV/cm)^3$) and simulation results at $\mu = 1279$ MeV/G and $K = 0.115\ G^{1/2} R_E$ for the October 2012 storm, with (a) last closed drift shell calculated using TS04 model; (b) PSD data from Van Allen Probes; (c–e) model results with "RD only," "RD + Hiss + Chorus" without realistic electron seed population, and "RD + Hiss + Chorus" with realistic electron seed population, respectively; and (f) *Dst* index.

2. DREAM3D Simulations

The DREAM3D diffusion model is based on a simplified version of the Fokker-Planck equation that ignores the cross terms ($D_{\alpha L}$, D_{pL}) between the drift shell, L^*, and the equatorial pitch angle, α, and momentum, p [*Schulz and Lanzerotti*, 1974]:

$$\frac{\partial f}{\partial t} = L^2 \frac{\partial}{\partial L}\left(\frac{D_{LL}}{L^2}\frac{\partial f}{\partial L}\right) + \frac{1}{p^2}\frac{\partial}{\partial p}\left(p^2 D_{pp}\frac{\partial f}{\partial p}\right) + \frac{1}{G}\frac{\partial}{\partial \alpha}\left(G D_{\alpha\alpha}\frac{\partial f}{\partial \alpha}\right) - \frac{f}{\tau} + \frac{1}{p^2}\frac{\partial}{\partial p}\left(p^2 D_{p\alpha}\frac{\partial f}{\partial \alpha}\right) + \frac{1}{G}\frac{\partial}{\partial \alpha}\left(G D_{\alpha p}\frac{\partial f}{\partial p}\right) \quad (1)$$

The model can be decoupled into a set of 1-D radial diffusion equations at fixed μ and K (first and second adiabatic invariants) and a set of 2-D pitch angle/momentum diffusion equations at fixed L^* that operate on the PSD as a function of (α, p). Specification of the diffusion coefficients is required to solve the equation. The radial diffusion coefficient, D_{LL}, is a function of *Kp* index from *Brautigam and Albert* [2000] (for the magnetic component) and *Brautigam et al.* [2005] (for the electric component). The pitch angle, momentum, and mixed diffusion coefficients ($D_{\alpha\alpha}$, D_{pp}, and $D_{\alpha p}$) are calculated following the method in *Glauert and Horne* [2005], using the wave normal angle distributions constructed from statistical results (*Li et al.* [2011] for chorus waves and *Agapitov et al.* [2013] for hiss), and the same statistical plasma density models as used in *Tu et al.* [2013]. Global wave intensity distributions in magnetic latitude (MLAT), magnetic local time (MLT), and L are required for the calculation. The computational volume of the 3-D diffusion model requires boundary conditions on six surfaces. The most important boundary conditions are the outer boundary condition at L_{max} and the low-energy boundary at $E_{min} = 100$ keV (which we call the electron seed population). More details on the standard setup of the DREAM3D model can be found in *Tu et al.* [2013].

Figure 1b shows the electron PSD data (in units of $(c/MeV/cm)^3$) calculated from the electron fluxes measured by the MagEIS (Magnetic Electron Ion Spectrometer) and REPT (Relativistic Electron-Proton Telescope) instruments aboard the two Van Allen Probes during the October 2012 event (6–11 October). They are for $\mu = 1279$ MeV/G and $K = 0.115\ G^{1/2}R_E$ (corresponding to approximately 2.0 MeV electrons with equatorial pitch angles of about 52° at $L^* = 4$ in a dipole). The PSD is evaluated using the Tsyganenko 04 storm time model (TS04) [*Tsyganenko and Sitnov*, 2005]. To simulate the electron dropout and buildup during the October 2012 event as shown in Figure 1b, three new modifications to the DREAM3D model have been implemented, all driven by event-specific conditions.

2.1. "Open" Boundary at $L_{max} = 11$ Combined With Short Electron Lifetimes Outside the Solar Wind-Driven Last Closed Drift Shell

The October 2012 storm was caused by a solar coronal mass ejection which significantly compressed the magnetopause and intensified the ring current around the Earth. The last closed drift shell (LCDS) of 90° equatorial pitch angle electrons in L^* is shown in Figure 1a, which is calculated under the TS04 model driven by event-specific solar wind conditions. It is compressed to inside $L^* = 6$ during both *Dst* dips, implying the possibility of strong magnetopause shadowing and outward radial diffusion of MeV electrons. Van Allen Probes are inside the LCDS during this event. In order to model outward radial diffusion of electrons to the compressed magnetopause and resolve its contribution to the observed fast electron dropout, we set the outer boundary at $L_{max} = 11$ (with $\partial f/\partial L = 0$ at $L_{max} = 11$), which is always greater than the LCDS during the event. Electrons outside the solar wind-driven LCDS (Figure 1a) are assumed to have a lifetime on the order of their drift period that is energy dependent. High-energy electrons with short drift periods will be lost quickly, causing a sharp gradient in PSD at the LCDS. The model results with radial diffusion only ($D_{\alpha\alpha}$, D_{pp}, and $D_{\alpha p}$ terms turned off) are shown in Figure 1c, for which the model initial condition (at 00 UT on 6 October) is derived from the Van Allen Probes PSD data. The timing and level of the electron dropout is reproduced by the model, proving the importance of outward radial diffusion to the observed electron dropout (consistent with the results in *Hudson et al*. [2014]). However, the simulated loss is not quite as deep in L^* as in the observations, which will be discussed in detail in section 3. The results in Figures 1d and 1e will be discussed below.

2.2. Event-Specific Chorus Waves

Typically, for the calculation of the pitch angle/momentum diffusion coefficients in the 3-D diffusion codes, empirical wave distributions derived from a statistical wave database are used [*Albert et al*., 2009; *Tu et al*., 2013]. For example, the global intensity distributions of chorus waves used in *Tu et al*. [2013] are statistically derived from the CRRES wave data, which are then binned in AE^* (the mean value of *AE* over the previous 1 h) [*Meredith et al*., 2003, 2004]. Based on this statistical model, the variation of the MLT-averaged chorus wave amplitude (actually the square root of the MLT-averaged wave intensity) near the equator is plotted in Figure 2b for the October 2012 event. Even though chorus wave amplitude varies with local time [*Meredith et al*., 2003], only MLT-averaged wave amplitude is used in our model since DREAM3D is drift-averaged which includes the effects of pitch angle/momentum diffusion averaged over electrons' drifts. To include the MLT-dependence of the scattering processes, a 4-D model which also resolves the drift-phase dependence of electron distribution is required. Since the empirical model is divided and averaged into three AE^* levels (<100, 100–300, and >300 nT, as marked in Figure 2c), the MLT-averaged wave amplitude in Figure 2b changes stepwise in time. The *AE* index reaches ~1000 nT during the event, much higher than the cutoff of the highest AE^* bin in the empirical model, calling into question the validity of the highly averaged statistical wave model during this active period. In situ observations of the chorus wave amplitude during the event are provided by the Van Allen Probes EMFISIS (Electric and Magnetic Field Instrument Suite and Integrated Science) instrument [*Kletzing et al*., 2013] (shown in Figure 2d). Strong chorus waves with amplitude greater than 100 nT are observed during both *Dst* dips. Even though high-quality wave measurements can be provided by the Van Allen Probes, they provide limited coverage in MLT and *L*. An event-specific wave model is needed that can provide the global distribution of chorus waves. Such a model has been developed by one of our coauthors, Yue Chen [*Chen et al*., 2014]. Since chorus waves are thought to be excited by substorm injected low-energy electrons, the model uses the low-energy precipitating electron flux (30–100 keV) measured by multiple NOAA satellites (covering a broad range of *L* and MLT) at low altitude as the proxy for global distribution of the near-equatorial chorus waves. Specifically, the precipitating electron flux measured at low altitude is fitted to the equatorial wave measurements made by EMFISIS to infer the chorus wave

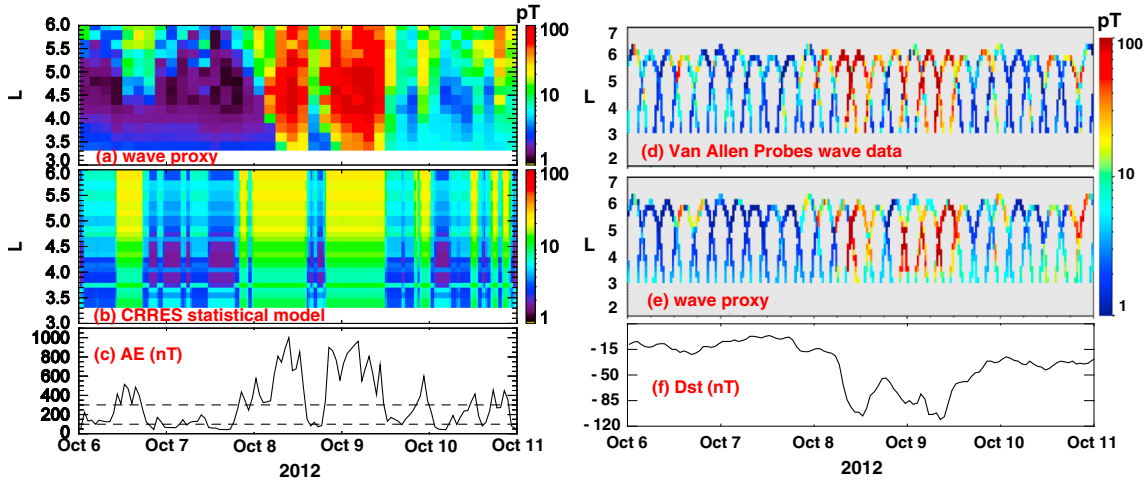

Figure 2. (a–c) Time and *L* distributions of the MLT-averaged chorus wave amplitude derived from the wave proxy in Figure 2a and the empirical model in Figure 2b, with the *AE* index plotted in Figure 2c. (d–f) Comparison of the chorus wave amplitude measured by the two Van Allen Probes in Figure 2d and derived from the proxy at Van Allen Probes' orbits in Figure 2e.

amplitude for this event. Figure 2e shows the chorus wave amplitudes calculated from the proxy at the Van Allen Probes' orbits, which exhibit striking resemblance to the data (comparing to Figure 2d). An alternative and more theoretical approach to obtaining global distribution of chorus waves has been published to use the ratio of precipitating to trapped electrons observed by NOAA satellites to derive the wave intensity [*W. Li et al.*, 2013]. That method has also been applied to the same event and validated against EMFISIS data. Future work is planned to compare the wave distributions derived from the two methods in more detail. Here we find that the MLT-averaged chorus wave amplitudes calculated from the proxy (shown in Figure 2a) can be >10 times higher than the statistical model (Figure 2b), leading to diffusion coefficients that are 100 times larger.

In order to simulate the strong enhancement of MeV electrons during the October 2012 event, we use the wave proxy to produce the event-specific chorus wave amplitude as a function of MLT, *L*, and time. Since the wave distribution in magnetic latitude (MLAT) cannot be resolved by the proxy, the MLAT dependence of chorus waves from the statistical model is used. The simulation results that include wave-particle interactions from this event-specific chorus wave model are shown in Figure 1d, which include radial diffusion and pitch angle/momentum diffusion from chorus and hiss. The hiss wave distribution is from the statistical model used in *Tu et al.* [2013] (also based on CRRES wave data). The results show some PSD enhancement toward the end of 8 October that is not present in the observations, but this enhancement is far less than the major enhancement observed on 9 October (Figure 1b). Local heating of radiation belt electrons to MeV energies needs not only strong waves but also a sufficient seed population to be heated. The seed population will be investigated in the next section.

2.3. Realistic Electron Seed Populations

In our previous work [*Tu et al.*, 2013] and the run in Figure 1d, the electron seed population, or low-energy boundary at $E_{min} = 100$ keV, is first set by the initial condition. For each time step the PSD at 100 keV is updated by the radial diffusion code but then held constant over the pitch angle/momentum diffusion step. Figure 3b shows the 100 keV electron flux versus time (black curve) from the model run in Figure 1d for electrons at $L^* = 4$ and with equatorial pitch angle $\alpha_{eq} = 50°$. The fluxes at higher energies are shown in different colors. These results show that the 100 s keV electrons are lost early on 8 October, and again early on 9 October, due to outward radial diffusion in the same manner as the MeV electrons. The absence of a replenishing seed population explains why the model does not produce enhancements of the MeV electrons even with strong chorus waves from the event-specific model (section 2.2). However, the dynamics of 100 s keV electrons produced by this model (Figure 3b) is not realistic since the dynamics of low-energy electrons are mainly controlled by convection and injection rather than diffusion [*Runov et al.*, 2012; *Ganushkina et al.*, 2013]. The real dynamics of the seed population are available directly from the Van Allen Probes data. The 100 keV to 2.5 MeV electron fluxes at $L^* = 4$ and $\alpha_{eq} = 50°$ measured by MagEIS and REPT are

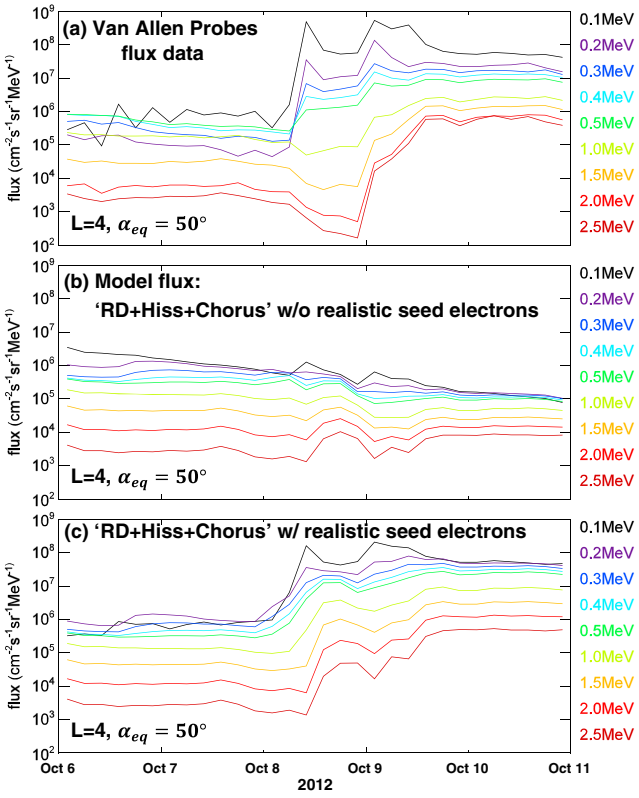

Figure 3. Observed (Figure 3a) and simulated (Figure 3b–c)variations of electron flux during the October 2012 storm, at $L = 4$ and $\alpha_{eq} = 50°$, and for electrons at different energies (0.1 to 2.5 MeV, shown in different colors). The model results are from the "RD + Hiss + Chorus" runs (b) without realistic electron seed population (same run with Figure 1d) and (c) with realistic electron seed population (same run with Figure 1e), respectively.

plotted in Figure 3a. The 1–2.5 MeV electron fluxes are observed to decrease early on 8 October then show an increase by the end of 8 October. However, the 100–500 keV electrons do not decrease early on 8 October but rather show an increase at this time, about a day earlier than the increase of MeV electrons, probably due to strong convection and injection from the plasma sheet [*Kress et al*., 2014]. This physics is not captured in our previous simulations.

In order to implement the realistic dynamics of the electron seed population in our model, the event-specific 100 keV electron flux observed by Van Allen Probes is used as the E_{min} boundary condition in the DREAM3D model, the third modification to the code made to model this event. With this data-driven E_{min} boundary condition, the new simulation results with radial diffusion and pitch angle/momentum diffusion from chorus and hiss are shown in Figure 3c for electron flux and in Figure 1e for electron PSD. Now the model reproduces a strong enhancement of MeV electrons, comparable to the data, with electron PSD peaked at $L^* \sim 4$, in the same location as the data. The simulation results demonstrate that both event-specific strong chorus waves and an accurate electron seed population are necessary for reproducing the remarkable enhancement of MeV electrons during the October 2012 event.

3. Discussion

Section 2 demonstrates the value of three different event-specific inputs and their profound effect on the DREAM3D model results: (1) specification of the time-dependent magnetopause/last closed drift shell based on solar wind conditions; (2) specification of the distribution of equatorial chorus wave intensity as a function of L, MLT, and time using LEO electron precipitation measurements; and (3) time-dependent measurements of the dynamic population of seed electrons measured in situ by the Van Allen Probes.

A major goal of the Living With a Star program strategy is to make the measurements required for a predictive understanding of the processes that drive severe space weather—rather than relying on statistical

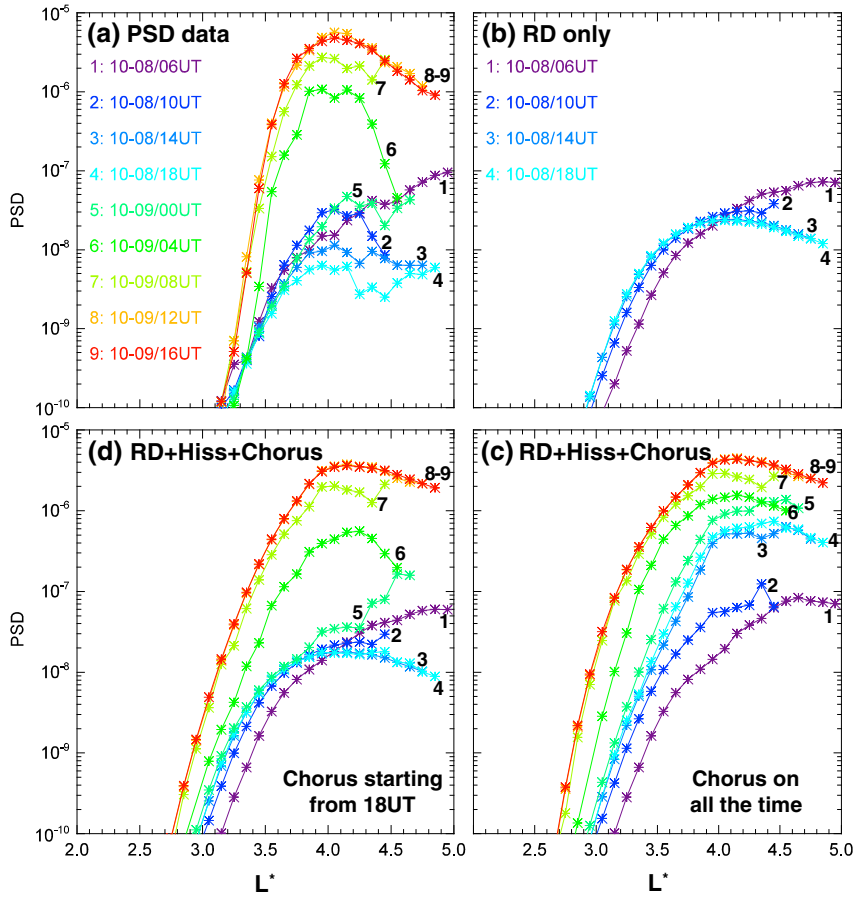

Figure 4. PSD versus L profiles at different times from the data and simulations at $\mu = 1279$ MeV/G and $K = 0.115\,G^{1/2}R_E$. Moving clockwise from (a) PSD data as shown in Figure 1b, (b–d) model results with "RD only" (same run with Figure 1c), "RD + Hiss + Chorus" (same run with Figure 1e), and "RD + Hiss + Chorus" but with chorus only turned on from 18 UT on 8 October, respectively.

distributions and geomagnetic indices. Here we look in more detail at the quantitative effects of this improved methodology. In Figure 4 we plot radial profiles of PSD observed by the two Van Allen Probes and calculated from different DREAM runs. The phase space densities plotted are for $\mu = 1279$ MeV/G and $K = 0.115\,G^{1/2}R_E$ and averaged over 4 h intervals (if both satellites measure the same L^* within each 4 h "snapshot," we average the data). The PSD data (Figure 4a) shows the fast dropout of radiation belt electrons from 06 to 18 UT on 8 October and the strong enhancement from 00 UT to 12 UT on 9 October. Figure 4b shows the PSD versus L^* from the simulation that includes only radial diffusion and loss to the time-dependent magnetopause. Here we only plot the first four snapshots (06–18 UT). We see that the model with radial diffusion alone reproduces the electron dropout outside $L^* = 4$, including the internal PSD peak observed in the data. This is clear evidence of electron losses due to outward radial diffusion combined with magnetopause shadowing [*Turner et al.*, 2012]. However, we find that the simulated loss is not as significant as in the data, in particular the large dropout at $L^* > 4.3$ from 06 to 10 UT on 8 October (snapshots #1–2) and the continuous loss over $L^* = 3.5$–4.5 from 10 to 18 UT on 8 October (snapshots #2–4). Possible explanations for this difference are that the last closed drift shell calculated using the TS04 model may not be accurate, or the empirical radial diffusion coefficient applied to the event may be too low, or other loss mechanisms also contribute, e.g., precipitation to the atmosphere.

The model run that includes local heating from chorus waves (using the global distribution derived from the proxy) is shown in Figure 4c (with panel order moving clockwise). The results show that local heating by the strong chorus waves during the first *Dst* dip overwhelms the electron loss from outward radial diffusion (Figure 1e). Thus, from 06 to 18 UT on 8 October (snapshots #1–4), the electron PSD inside $L^* = 4.5$ does not show a decrease, as in the data, but rather shows an early increase. As discussed above, this discrepancy

could be explained by loss mechanisms that are not in the model. Whatever the cause, the difference between the model and the observations prior to 9 October (snapshots #1–4) could affect the DREAM3D results on 9 October (snapshots #5–9). One way to test this possibility would be to reinitialize the simulation at 18 UT on 8 October using Van Allen observations. Another (more difficult) test is to include the entire simulation run but to "turn off" chorus during the observed flux dropout period, i.e., prior to 18 UT on 8 October. The simulation results from this model are shown in Figure 4d, which show that now, the electron dropouts produced by outward radial diffusion (snapshots #1–4) are retained, as is the fast and large PSD enhancement by chorus heating during the second *Dst* dip (snapshots #5–8). We conclude that the dramatic enhancement during the second *Dst* dip is explained by local acceleration of the seed population, but to fully explain the dynamics earlier on 8 October we need either an additional loss mechanism or better understanding of why the chorus waves are less effective in acceleration. Not only does the model produce results that are strikingly similar to the observations but also enables more complete understanding of the dynamics by examining contributions of individual processes to the overall radiation belt response.

4. Conclusions

The results presented here are the first using the DREAM3D diffusion model with event-specific chorus wave and seed population inputs to simulate a very complex and dynamic radiation belt electrons event observed by the Van Allen Probes. Without utilizing adjustable parameters, the model results quantitatively reproduce the strong electron enhancement during the second *Dst* dip (both the enhancement level and peak *L* location) and qualitatively explain the electron dropout during the first *Dst* dip, which clearly demonstrates the importance of event-specific inputs and boundary conditions. Utilizing model runs with different inputs and assumptions we can evaluate the effects of individual processes as well as the delicate interplay of processes that produces the net changes in the radiation belts. We show that in order to explain the very different behavior in the two dips, diffusion in all three dimensions (energy, pitch angle, and L^* shell) coupled with realistic, event-specific data inputs and boundary conditions is required. Specifically, a realistic outer radial boundary (last closed drift shell) is required to accurately capture magnetopause losses, even though additional loss process is needed to better reproduce the observed dropout; the global distribution of chorus waves derived from precipitating electrons measured by multiple NOAA satellites is required to accurately capture the local heating process; and accurate specification of the dynamic seed population from Van Allen observations is required to reproduce the amplitude of the PSD changes. In contrast, models with reduced dimensionality, models that derive the seed population from inward radial diffusion, and models that utilize statistical wave amplitudes parameterized by *AE* all fail to reproduce one or more of the major features observed in the October 2012 event.

Acknowledgments

We gratefully acknowledge the support of the U.S. Department of Energy through the LANL Laboratory Directed Research and Development (LDRD) Program for this work. This work was partially supported by RBSP-Energetic Particle Composition and Thermal Plasma Suite funding provided by the Johns Hopkins University Applied Physics Laboratory (JHU/APL) contract 967399 and NASA's Prime contract NAS5-01072. We also acknowledge the PI and instrument team of NOAA/POES SEM-2 for providing data from multiple NOAA satellites.

The Editor thanks Tsutomu Nagatsuma and an anonymous reviewer for their assistance in evaluating this paper.

References

Agapitov, O., A. Artemyev, V. Krasnoselskikh, Y. V. Khotyaintsev, D. Mourenas, H. Breuillard, M. Balikhin, and G. Rolland (2013), Statistics of whistler-mode waves in the outer radiation belt: Cluster STAFF-SA measurements, *J. Geophys. Res. Space Physics*, *118*, 3407–3420, doi:10.1002/jgra.50312.

Albert, J. M., N. P. Meredith, and R. B. Horne (2009), Three-dimensional diffusion simulation of outer radiation belt electrons during the 9 October 1990 magnetic storm, *J. Geophys. Res.*, *114*, A09214, doi:10.1029/2009JA014336.

Brautigam, D. H., and J. M. Albert (2000), Radial diffusion analysis of outer radiation belt electrons during the 9 October 1990 magnetic storm, *J. Geophys. Res.*, *105*, 291–309, doi:10.1029/1999JA900344.

Brautigam, D. H., G. P. Ginet, J. M. Albert, J. R. Wygant, D. E. Rowland, A. Ling, and J. Bass (2005), CRRES electric field power spectra and radial diffusion coefficients, *J. Geophys. Res.*, *110*, A02214, doi:10.1029/2004JA010612.

Chen, Y., G. D. Reeves, and R. H. W. Friedel (2007), The energization of relativistic electrons in the outer Van Allen radiation belt, *Nat. Phys.*, *3*(9), 614–617, doi:10.1038/nphys655.

Chen, Y., G. D. Reeves, R. H. W. Friedel, and G. S. Cunningham (2014), Global time-dependent chorus maps from low-earth-orbit electron precipitation and Van Allen Probes data, *Geophys. Res. Lett.*, doi:10.1002/2013GL059181.

Elkington, S. R., M. K. Hudson, and A. A. Chan (2003), Resonant acceleration and diffusion of outer zone electrons in an asymmetric geomagnetic field, *J. Geophys. Res.*, *108*(A3), 1116, doi:10.1029/2001JA009202.

Ganushkina, N. Y., O. A. Amariutei, Y. Y. Shprits, and M. W. Liemohn (2013), Transport of the plasma sheet electrons to the geostationary distances, *J. Geophys. Res. Space Physics*, *118*, 82–98, doi:10.1029/2012JA017923.

Glauert, S. A., and R. B. Horne (2005), Calculation of pitch angle and energy diffusion coefficients with the PADIE code, *J. Geophys. Res.*, *110*, A04206, doi:10.1029/2004JA010851.

Horne, R. B., and R. M. Thorne (1998), Potential waves for relativistic electron scattering and stochastic acceleration during magnetic storms, *Geophys. Res. Lett.*, *25*(15), 3011–3014, doi:10.1029/98GL01002.

Horne, R. B., R. M. Thorne, S. A. Glauert, J. M. Albert, N. P. Meredith, and R. R. Anderson (2005), Timescale for radiation belt electron acceleration by whistler mode chorus waves, *J. Geophys. Res.*, *110*, A03225, doi:10.1029/2004JA010811.

Hudson, M. K., et al. (2000), Increase in relativistic electron flux in the inner magnetosphere: ULF wave mode structure, *Adv. Space Res.*, *25*, 2327–2337.

Hudson, M. K., D. N. Baker, J. Goldstein, B. T. Kress, J. Paral, F. R. Toffoletto, and M. Wiltberger (2014), Simulated Magnetopause Losses and Van Allen Probe Flux Dropouts, *Geophys. Res. Lett.*, doi:10.1002/2014GL059222.

Kletzing, C. A., et al. (2013), The Electric and Magnetic Field Instrument Suite and Integrated Science (EMFISIS) on RBSP, *Space Sci. Rev.*, *179*, 127–181, doi:10.1007/s11214-013-9993-6.

Kress, B. T., M. K. Hudson, and J. Paral (2014), Rebuilding of the Earth's outer electron belt during 8–10 October 2012, *Geophys. Res. Lett.*, *41*, doi:10.1002/2013GL058588.

Li, W., J. Bortnik, R. M. Thorne, and V. Angelopoulos (2011), Global distribution of wave amplitudes and wave normal angles of chorus waves using THEMIS wave observations, *J. Geophys. Res.*, *116*, A12205, doi:10.1029/2011JA017035.

Li, W., B. Ni, R. M. Thorne, J. Bortnik, J. C. Green, C. A. Kletzing, W. S. Kurth, and G. B. Hospodarsky (2013), Constructing the global distribution of chorus wave intensity using measurements of electrons by the POES satellites and waves by the Van Allen Probes, *Geophys. Res. Lett.*, *40*, 4526–4532, doi:10.1002/grl.50920.

Li, X., et al. (2013), First results from CSSWE CubeSat: Characteristics of relativistic electrons in the near-earth environment during the October 2012 magnetic storms, *J. Geophys. Res. Space Physics*, *118*, 6489–6499, doi:10.1002/2013JA019342.

Meredith, N. P., R. B. Horne, R. M. Thorne, and R. R. Anderson (2003), Favored regions for chorus-driven electron acceleration to relativistic energies in the Earth's outer radiation belt, *Geophys. Res. Lett.*, *30*(16), 1871, doi:10.1029/2003GL017698.

Meredith, N. P., R. B. Horne, R. M. Thorne, D. Summers, and R. R. Anderson (2004), Substorm dependence of plasmaspheric hiss, *J. Geophys. Res.*, *109*, A06209, doi:10.1029/2004JA010387.

Morley, S. K., et al. (2010), Dropouts of the outer electron radiation belt in response to solar wind stream interfaces: Global positioning system observations, *Proc. R. Soc. A*, *466*, 3329–3350, doi:10.1098/rspa.2010.0078.

Reeves, G. D., D. N. Baker, R. D. Belian, J. B. Blake, T. E. Cayton, J. F. Fennell, R. H. W. Friedel, M. M. Meier, R. S. Selesnick, and H. E. Spence (1998), The global response of relativistic radiation belt electrons to the January 1997 magnetic cloud, *Geophys. Res. Lett.*, *25*(17), 3265, doi:10.1029/98GL02509.

Reeves, G. D., K. L. McAdams, and R. H. W. Friedel, T. P. O'Brien (2003), Acceleration and loss of relativistic electrons during geomagnetic storms, *Geophys. Res. Lett.*, *30*(10), 1529, doi:10.1029/2002GL016513.

Reeves, G. D., et al. (2013), Electron acceleration in the heart of the Van Allen radiation belts, *Science*, *341*, 991–994, doi:10.1126/science.1237743.

Roederer, J. G. (1970), *Dynamics of Geomagnetically Trapped Radiation*, Springer, New York.

Runov, A., V. Angelopoulos, and X.-Z. Zhou (2012), Multipoint observations of depolarization front formation by magnetotail reconnection, *J. Geophys. Res.*, *117*, A05230, doi:10.1029/2011JA017361.

Schulz, M., and L. Lanzerotti (1974), *Particle Diffusion in the Radiation Belts*, Springer, New York.

Selesnick, R. S. (2006), Source and loss rates of radiation belt relativistic electrons during magnetic storms, *J. Geophys. Res.*, *111*, A04210, doi:10.1029/2005JA011473.

Selesnick, R. S., and J. B. Blake (2000), On the source location of radiation belt relativistic electrons, *J. Geophys. Res.*, *105*(A2), 2607–2624, doi:10.1029/1999JA900445.

Shprits, Y., M. Daae, and B. Ni (2012), Statistical analysis of phase space density buildups and dropouts, *J. Geophys. Res.*, *117*, A01219, doi:10.1029/2011JA016939.

Thorne, R. M., et al. (2013), Rapid local acceleration of relativistic radiation-belt electrons by magnetospheric chorus, *Nature*, *504*, 411–414, doi:10.1038/nature12889.

Tsyganenko, N. A., and M. I. Sitnov (2005), Modeling the dynamics of the inner magnetosphere during strong geomagnetic storms, *J. Geophys. Res.*, *110*, A03208, doi:10.1029/2004JA010798.

Tu, W., X. Li, Y. Chen, G. D. Reeves, and M. Temerin (2009), Storm-dependent radiation belt electron dynamics, *J. Geophys. Res.*, *114*, A02217, doi:10.1029/2008JA013480.

Tu, W., R. Selesnick, X. Li, and M. Looper (2010), Quantification of the precipitation loss of radiation belt electrons observed by SAMPEX, *J. Geophys. Res.*, *115*, A07210, doi:10.1029/2009JA014949.

Tu, W., G. S. Cunningham, Y. Chen, M. G. Henderson, E. Camporeale, and G. D. Reeves (2013), Modeling radiation belt electron dynamics during GEM challenge intervals with the DREAM3D diffusion model, *J. Geophys. Res. Space Physics*, *118*, 6197–6211, doi:10.1002/jgra.50560.

Turner, D. L., Y. Shprits, M. Hartinger, and V. Angelopoulos (2012), Explaining sudden losses of outer radiation belt electrons during geomagnetic storms, *Nat. Phys.*, *8*, 208–212, doi:10.1038/nphys2185.